NeuroImage 322 (2025) 121562

Contents lists available at ScienceDirect

NeuroImage

journal homepage: www.elsevier.com/locate/ynimg

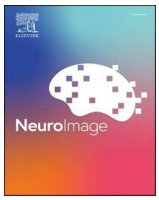

The Adolescent functional connectome is dynamically controlled by a sparse core of cognitive and topological hubs

Jethro Lim [a], Ilias Mitrai [b], Prodromos Daoutidis [c], Catherine Stamoulis [a,d,*]

[a] Department of Pediatrics, Division of Adolescence and Young Adult Medicine, Boston Children's Hospital, Boston, MA 02115, USA
[b] McKetta Department of Chemical Engineering, The University of Texas at Austin, Austin, TX 78712, USA
[c] Department of Chemical Engineering and Material Sciences, University of Minnesota, Minneapolis, MN 55455, USA
[d] Department of Pediatrics, Harvard Medical School, Boston, MA 02115, USA

ARTICLE INFO

Keywords:
Adolescence
Brain development
Resting-state networks
Network controllability
Feedback control
Sparsity

ABSTRACT

Fundamental mechanisms that control the brain's ability to dynamically respond to cognitive demands are poorly understood, especially during periods of accelerated neural and cognitive maturation, such as adolescence. Using a sparsity-promoting feedback control framework we investigated the controllability of the adolescence functional connectome. Critical feedback costs associated with a region's control action on itself and the rest of the brain were estimated using resting-state fMRI data from an early longitudinal sample in the Adolescent Brain Cognitive Development (ABCD) study (n = 1394; median (IQR) age = 10.1 (1.1) years at baseline and 12.1 (1.1) years at follow-up). A highly reproducible, core set of predominantly highly connected regions retained their control action over the connectome under high feedback costs. They included posterior visual areas, retrosplenial cortex, cuneus and precuneus, superior parietal lobule, ventral temporal cortex and dorsolateral and lateral prefrontal cortices, i.e., both developed and developing brain regions. These regions were central to the topological organization of the connectome, consistently engaged during spontaneous coordination of resting-state networks, and overlapped with cognitive and topological brain hubs that play ubiquitous roles in cognitive function and the organization of the connectome. Also, most received (integrated) and distributed approximately equal amounts of neural information. These regions' control action was developmentally stable, i.e., critical feedback costs did not change significantly during puberty, suggesting that, despite ongoing maturation and topological changes in the adolescent brain, fundamental mechanisms of system controllability may be fairly well developed to facilitate information processing and response to cognitive demands.

1. Introduction

The brain's ability to respond to myriads of external inputs and complex cognitive demands critically depends on its capacity to transition between states (physiological, cognitive, topological and/or dynamic), which are accompanied by specific patterns of interaction between its regions (Myer-Lyndenberg et al., 2002; Deco et al., 2011; Cocchi et al., 2013; Tognoli and Kelso, 2014; Breakspear, 2017; Vidaurre et al., 2017; Shine and Poldrack, 2018; Taghia et al., 2018; Kringelbach and Deco, 2020). However, the underlying mechanisms that regulate (control) these state transitions are incompletely understood (Hansen et al., 2015).

Recent work has used tools from control theory to elucidate the brain's controllability (the ability to effect transitions from one network state to another). Some of these tools have been applied to graph (network) representations of brain circuits, in order to investigate the brain's response to control inputs in specific regions (Pasqualetti et al., 2014; Gu et al., 2015; Betzel et al., 2016; Lee et al., 2019; Parkes et al., 2023). Most brain studies using control theoretic tools have used an open-loop framework, i.e., one where the control action does not adapt based on feedback from the system output, and have shown that state transitions may be controlled by a small set of brain regions that are active in a particular state (Gu et al., 2015, 2017). In addition, highly connected regions form a 'core' network (van den Heuvel and Sporns, 2011), that supports the minimization of control energy (i.e., the overall control effort, quantified by the values of the control inputs necessary to enforce a transition) that is required for shifting the brain from one dynamic state to another (Betzel et al., 2016), and optimize cognitive

* Corresponding author at: Department of Pediatrics, Division of Adolescence and Young Adult Medicine, Boston Children's Hospital, Boston, MA 02115, USA.
E-mail address: caterina.stamoulis@childrens.harvard.edu (C. Stamoulis).

https://doi.org/10.1016/j.neuroimage.2025.121562
Received 28 May 2025; Received in revised form 27 October 2025; Accepted 28 October 2025
Available online 29 October 2025

function (Cui et al., 2020). Within this framework, control energy has also been correlated with temporal changes in functional connectivity (Deng et al., 2022). Recent translational work has also used the open-loop control framework to elucidate changes in brain dynamics and controllability associated with neuropsychiatric disorders, such as schizophrenia and psychosis, where networks lose their efficiency (network dynamics are harder to control, and thus the required control effort increases) as the brain remains in high-energy- states (Braun et al., 2021; Zoller et al., 2021; Parkes et al., 2021). Network controllability has also been examined as a predictor of language recovery after stroke (Wilmskoetter et al., 2022).

In contrast to the open-loop framework, a closed-loop control framework assumes that internal processes control the system's dynamics, and feedback information drives adjustments to the controller's action, to optimize system performance. This type of control framework has been used in brain stimulation, brain-machine interface and neurofeedback (Wright et al., 2016; Zrennar et al., 2016; Sitaram et al., 2017; Zhang et al., 2023). These applications specifically seek to optimize either the brain's dynamic response (e.g., to stimulation) or motor behaviors through feedback signals. For example, motor learning critically depends on feedback information which is used to progressively minimize errors associated with learning a new motor task. Brain-machine interfaces also depend on feedback information to optimize machine performance.

Few, if any, studies have used a closed-loop control framework to address fundamental questions on how brain dynamics are controlled by internal latent processes that are impossible to measure in the intact human brain. Such latent processes, which are inherently based on feedback, are not accounted for in an open-loop framework. For example, the brain's metabolic demands depend on its activity, and thus on feedback information related to neural activation and coordination. Our study is motivated by this important gap in knowledge, especially in the context of the developing brain. To date, mechanisms and processes driving the optimization of neural circuitry and brain dynamics, which are likely controlled by biochemical processes that develop in parallel with the brain, are incompletely understood.

A closed-loop control framework that accounts for the topological organization of the brain, which is characterized by community structure and sparsity (Eavani et al., 2015), provides a powerful modeling approach for addressing this fundamental question. The adult (developed) brain's small-world and rich-club topological organization facilitates efficient local (domain-specific) computation and global (domain-general) integration through sparse long-range connections (van den Heuvel and Sporns, 2011; Bassett and Bullmore, 2017). Therefore, a sparsity-promoting, feedback control framework is conceptually appropriate for studying the controllability of brain networks (Lin et al., 2013; Constantino et al., 2019). In such a framework, the controller's action is spatially sparse, and is optimized through balance between performance and feedback costs, a process that is likely well-aligned with the action of biological mechanisms underlying the controllability of brain networks. In recent work, we have applied this control framework to investigate the controllability of macaque structural networks (Mitrai, et al. 2021) and in preliminary studies of human functional networks in adolescence (Mitrai et al., 2023; Lim et al., 2024).

In this study, we used this framework to address the fundamental question of controllability in developing brain networks in adolescence, a sensitive period of heightened maturation (and profound reorganization of brain circuits that includes elimination of redundant connections and selective strengthening of remaining ones). We hypothesized that despite its suboptimal and evolving organization, just like the adult brain, the adolescent connectome is controlled by a relatively sparse set of regions that play a critical role in its dynamics. To test this hypothesis, we applied a sparsity-promoting feedback control framework to intrinsic networks from a sample of ~1400 adolescents from the Adolescent Brain Cognitive Development (ABCD) study (Casey et al, 2018) with early longitudinal neuroimaging data (baseline (ages ~9–10 y) and two-year follow-up (ages ~11–12 y), spanning pre/early to late puberty. We focused on two sets of critical costs, a) those associated with self-control (i.e., cost at which a region's dynamics are controlled only by the action of that region), and b) high feedback costs at which a region retains (or loses) its control action on the brain. The latter set was used to test the hypothesis that controllability of brain dynamics depends on small set of regions that maintain their control action even at high feedback costs. To elucidate the roles of network topology on controllability, we then investigated associations between feedback control costs and regional connectome characteristics, including connectedness, information flow, and dynamics. Finally, we assessed relationships between region-specific feedback control costs and demographic and other participant characteristics, especially pubertal stage, in order to elucidate the impact of brain development on the connectome's internal control.

2. Methods

The study was approved by the Boston Children's Hospital Institutional Review Board.

2.1. Sparsity promoting feedback framework

The control framework used in the study is described in detail in prior work (Lin et al., 2013) Mitrai et al., 2023). Briefly, the brain is represented as a linear time-invariant system described by:

$$d\mathbf{x}(t)/dt = \mathbf{A}\mathbf{x}(t) + \mathbf{B_1}\mathbf{u}(t) + \mathbf{B_2}\mathbf{d}(t) \quad (1)$$

where $\mathbf{x}$ is the dynamic system state, $\mathbf{u}$ is the control input (in this context the control action at each region)), $\mathbf{d}$ are the external input(s) to the system, $\mathbf{A}$ describes the internal dynamic behavior of the system, and $\mathbf{B_1}$ and $\mathbf{B_2}$ are matrices that map the control and external inputs to the system state. The control input is related to the state by:

$$\mathbf{u}_{\{i\}} = -\sum_{\{j=1\}}^{N} \mathbf{K}_{\{i,j\}}\mathbf{x}_{\{j\}} \quad (2)$$

where $\mathbf{K}$ is the feedback gain matrix, and N the total number of regions. Each element $\mathbf{(i,j)}$ of $\mathbf{K}$ represents the feedback control action that region $\mathbf{j}$ exerts on region $\mathbf{i}$, i.e., this matrix captures the relation between the control action at region i and the dynamic state of other regions. $\mathbf{K}$ represents the required exchange of information between regions when the control action is estimated. It is the target of optimization (which aims to balance control and feedback costs) and is obtained by penalizing its non-zero entries while maximizing control performance. The optimization thus aims to:

$$\text{minimize}_K \text{trace}(\mathbf{P}(\mathbf{K})) + \mathbf{p}\text{card}(\mathbf{K}) \quad (3)$$

where $\mathbf{p}$ captures the feedback cost, card(.) is cardinality, and $\mathbf{P(K)}$ is related to $\mathbf{A}$ and $\mathbf{K}$ by:

$$(\mathbf{A}-\mathbf{K})\mathbf{P} + \mathbf{P}(\mathbf{A}-\mathbf{K})^{\mathbf{T}} + (\mathbf{I}+\mathbf{K}^{\mathbf{T}}\mathbf{K}) = \mathbf{0} \quad (4)$$

As $\mathbf{p}$ increases, the cardinality of K decreases and thus its sparsity increases.

This optimization problem was solved using the alternating direction method of multipliers (ADMM) algorithm (Boyd et al., 2011; (Lin et al., 2013)), restricting the range of $\mathbf{p}$ values to $p \in [10^{-4}, 30]$. The upper bound was selected empirically, by examining the number of regions retaining their control action as p increases, i.e., the cardinality of $\mathbf{K}$ (see Figure S6 for an example). At $p > \sim 20$, the cardinality of K remained almost constant. Within the selected range, two critical values were of specific interest, p at which a region's control action does not depend on any other region (i.e., the feedback gain matrix becomes diagonal), and a critical transition p value at which a region no longer exerts its control action over the network (or retains its action if p has reached the upper limit). Figure S1 summarizes the control analysis pipeline.

2.2. Participants

Resting-state (rs) fMRI data from 1394 youth (53.7 % female, 53.7 % white non-Hispanic, 21.7 % Hispanic) in the ABCD study were analyzed. Median age (inter-quartile range (IQR)) was 10.1 (1.1) years at baseline and 12.1 (1.1) years at follow-up. Detailed participant characteristics are provided in Table 1. Youth with a diagnosis of Attention Deficit Hyperactivity Disorder (ADHD), Autism Spectrum Disorder (ASD), or a neuropsychiatric disorder (including bipolar and psychotic disorders and schizophrenia) were excluded, as these have been associated with abnormally connected brain circuits and aberrant neural dynamics (van den Heuvel and Fornito, 2014; Kottaram et al., 2019; Cherkassky et al., 2006; Assaf et al., 2010; Konrad et al., 2010; Chase et al., 2016). Also, youth with clinical findings in their structural MRI were excluded (Brooks et al., 2021). All participants had early longitudinal data (i.e., two assessments, at baseline and 2-year follow-up). The sample was selected based on a requirement of two high-quality rs-fMRI runs (each 5 min long) at both assessments for replication analyses. Data quality in a particular run was assessed based on median connectivity of the entire connectome (which is inherently low at rest) and the number of frames censored for motion (based on a displacement threshold of 0.3 mm). In the selected runs, median percent of frames censored for motion was 0.8 %−1.3 % at baseline, and 0.5 %−0.8 % at follow-up. All analyses were adjusted for the time of fMRI scan (rounded to the nearest hour, and thus represented by a 0–23 variable), to account for differences in topological parameters resulting from differences in the time of day at which participants were scanned (Hu et al., 2023), and percent of frames censored for motion (Brooks et al., 2021).

Table 1
Participant characteristics at baseline and follow-up.

		Baseline (N = 1394)	Two-year follow-up (N = 1394)
Age (Median (IQR)); years		10.1 (1.1)	12.1 (1.1)
Sex	**Male**	644 (46.3 %)	
	Female	748 (53.7 %)	
Race-Ethnicity	**White Non-Hispanic**	748 (53.7 %)	
	Black Non-Hispanic	173 (12.4 %)	
	Asian Non-Hispanic	30 (2.2 %)	
	Other Non-Hispanic	137 (9.8 %)	
	Hispanic	303 (21.7 %)	
	Missing	3 (0.2 %)	
BMI (Median (IQR))	**Raw Score**	17.49 (4.03)	19.04 (5.15)
	Z-Score	−0.33 (1.00)	−0.33 (1.07)
	Missing	4	7
Pubertal Stage	**Pre-Puberty**	673 (48.3 %)	242 (17.4 %)
	Early Puberty	316 (22.7 %)	282 (20.2 %)
	Mid-Puberty	343 (24.6 %)	471 (33.8 %)
	Late/Post-Puberty	26 (1.9 %)	327 (23.5 %)
	Missing	36 (2.6 %)	72 (5.2 %)
Family Income	**<25,000**	146 (10.5 %)	123 (8.9 %)
	25,000 −49,999	191 (13.7 %)	165 (11.8 %)
	50,000–99,999	341 (24.5 %)	347 (24.9 %)
	100,000–199,999	424 (30.4 %)	446 (32.0 %)
	>=200,000	193 (13.8 %)	225 (16.1 %)
	Missing	99 (7.1 %)	88 (6.3 %)

2.3. fMRI data processing

All analyzed rs-fMRI data (from the ABCD release 4.0) had been minimally preprocessed by the Data Analysis, Informatics & Resource Center (DAIRC; Hagler et al., 2019), and were further processed using the Next-Generation Neural Data Analysis (NGNDA) pipeline. Processing details are provided in Brooks et al., 2021. Briefly, each participant's fMRI data were corrected for motion, co-registered to their T1 structural MRI, normalized to NMI space, denoised to suppress artifacts, and harmonized across scanners (fMRI had been acquired at 21 sites of the ABCD, using 3.0T Siemens, GE and Philips scanners). Repetition time (TR) was 0.8 s across scanners. Voxel-level data were parcellated using 3 atlases (cortical, subcortical and cerebellar), resulting in 1088 parcels (1000 cortical, 54 subcortical and 34 cerebellar; (Schaefer et al., 2018; Tian et al 2020; Diedrichsen et al., 2009)). To facilitate computationally tractable control analyses, the higher resolution data (1088 parcels) were then further downsampled to 100 regions based on anatomical boundaries and the delineation of large resting-state networks identified in (Yeo et al., 2011). To assess the sensitivity of estimated control costs to the spatial resolution of the data parcellation, in secondary analyses a second higher-resolution parcellation using 300 cortical parcels (also based on Schaefer et al., 2018) was used, resulting in a total of 388 regions.

Connectivity matrices were estimated using peak pairwise signal cross-correlation (in the range 0–1) as a measure of connection strength. Each matrix was thresholded using assessment-specific, cohort-wide statistical thresholds (the same threshold was used for both runs within each assessment). Given that the brain is overall weakly correlated at rest, with a relatively low number of active functional connections, a threshold equal to median + 1.5*IQR (moderate outlier threshold) was selected. Values below the given threshold were set equal to 0, resulting in relatively sparse adjacency matrices. There is currently no clear consensus on an optimal approach for identifying true functional connections from noisy connectivity matrices that include spurious edges. Our approach is based on statistical considerations, preserves the strongest functional connections (and thus those most likely overlapping with their structural constraints), and allows for comparisons between brains.

To assess the impact of thresholding on estimated control costs, secondary analyses were also conducted using a less conservative threshold, corresponding to the cohort-wide 75th percentile of cross-correlation values. This threshold is approximately equal to brain-specific proportional thresholds that retain 25 % of connections, and a percolation-based threshold estimated independently (Brooks et al., 2021)).

Before solving the control problem, each adjacency matrix **A** was normalized using its maximum eigenvalue λ_{max}, to ensure that at time $t = 0$ it represented a stable dynamic system:

$$A_{norm} = A\frac{1}{\lambda_{max}(A)+1} - I \quad (5)$$

2.4. Regional topological characteristics

2.4.1. Net information flow

To assess the direction of information transfer between pairs of regions (their effective connectivity), a variant of the Granger causality method was used (Chen et al., 2019; Geweke, 1982), which is based on estimating the optimal lag between two time series, obtained by minimizing the Akaike Information Criterion (AIC) value. Two test statistics were further considered, the $F_{i->j}$ value, representing a directed edge from region i to region j, and the corresponding p-value, used to assess the significance of the directionality. Only significant directed regions were considered. Net flow was calculated as the difference between information in and out of a region. This approach was selected following comparisons with other methods, in particular phase transfer entropy

(PTE; Lobier et al., 2013), which lead to statistically (and topologically) similar effective connectivity matrices.

2.4.2. Regional connectedness (node degree) and dynamic engagement

Degree was estimated from the adjacency matrix as the total number of a region's connections (edges). In addition, time-dependent adjacency matrices (estimated by thresholding corresponding correlation matrices, obtained using a 20-point sliding window (~16 s) with a one-point increment) were used to estimate each region's time-varying degree (Lim, et al., 2025). Time points corresponding to frames censored for motion were then excluded, and each region's degree was normalized by the brain-wide maximum estimated degree (across regions and time points). If a region's (normalized) degree was greater or equal to a threshold of 0.5, the region was considered *engaged*. Frequency of region engagement was defined as the number of time points in which a region's degree met or exceeded this threshold.

2.5. Statistical analysis

Linear mixed effects regression models were developed to investigate associations between estimated feedback control costs and pubertal stage. The Pubertal Development Scale (Petersen, 1988) is used by the ABCD study to measure pubertal stage. Parents are asked to answer questions on their child's physical changes, including skin and body hair changes, height spurt, menstruation, breast development, changes in voice (deepening), and facial hair. These responses are added and then categorized on a scale 1 (pre-puberty) to 5 (post-puberty). In this study, since a very small number of youth (<1 %) were in post-puberty, for statistical modeling purposes they were combined with those in late puberty in a single category (= 4).

Models included adjustments for sex, race/ethnicity (dichotomized as white non-Hispanic vs racial/ethnic minorities, given small samples and thus limited statistical power of individual racial categories), family income and BMI z-score (stratified by sex). These parameters were also independently examined in models to identify links between demographic and other participant characteristics and estimated costs. Models combined data from both baseline and two-year follow-up, and a random intercept and slope were included in the models to account for each participant's repeated measurements. All statistical analyses accounted for sampling differences across the 21 ABCD sites, using propensity weights provided by the ABCD. All analyses assumed a significance level $\alpha = 0.05$, and p-values were corrected for False Discovery Rate (FDR; (Benjamini and Hochberg, 1995)).

2.6. Similarity of spatial cost distributions

To compare the spatial distributions of control costs across resolutions, between runs, and between thresholds, two similarity measures were estimated, cosine similarity and the Barroni-Urbani (BU) coefficient. No resampling was necessary when comparisons were made at the same resolution. However, across the two resolutions of interest (100 vs 388 regions), estimated costs were mapped back to the original 1088 regions. Then, pairs of vectors (each with 1088 elements) were compared, using cosine similarity. In addition, to specifically compare the spatial patterns of regions associated with high control costs at the two resolutions, brain- and resolution-specific thresholds were imposed on weighted vectors, to binarize them and compare them using the BU coefficient. Two thresholds were selected, corresponding to the 75th and the 90th percentile of control costs at which regions no longer maintain their control action over the network.

3. Results

3.1. Distribution of feedback control costs across participants and brain regions

We first examined the consistency (across the cohort), of the spatial distribution of costs at which individual regions maintained their control action over the network (or lost their action if costs are lower than the upper limit of the examined range). These costs are shown in Fig. 1, for baseline (a) and 2-year follow up (b), and were estimated from the best-quality fMRI run, and adjacency matrices thresholded based on the moderate outlying peak cross-correlation value. For each analyzed region, the figure also shows median (over participants) control costs (bar graph below the heat map) and median degree (bar graph above the heat map). Across participants, the highest costs were associated with regions of the visual networks and the frontoparietal control network, both at baseline and the two-year follow-up, and did not vary substantially with age, within or across assessments. Corresponding findings for feedback costs at which regions become self-controlled (i.e., their dynamics no longer depend on the control action of other regions) are shown in supplemental Figure S2.

The corresponding group-level (median) spatial distributions of costs associated with self-control and loss of control action, respectively, are shown in Fig. 2. Within the range of feedback costs associated with self-control ([min, max] = [<0.01, 0.30]), higher values were estimated in bilateral posterior areas overlapping with the visual peripheral network, bilateral superior parietal lobules (SPL), and bilateral dorsolateral prefrontal areas that partly overlapped with the salience, but more extensively with the frontoparietal control and default-mode (DM) networks. Within the range of feedback costs associated with regions maintaining (or losing) their control action over the network (median over participants of [min, max] = [8.58, 30.0]), the highest critical feedback costs were estimated in left dorsolateral prefrontal cortical areas, overlapping with the frontoparietal control network. In addition, high feedback costs were estimated in other bilateral frontal regions, overlapping with the DM and salience networks, as well as in posterior visual peripheral areas, bilateral SPL, the left ventral temporal area (part of the inferior temporal gyrus), overlapping with the frontoparietal control network), the right precuneus and right retrosplenial cortex. Overall, most of these regions had high critical feedback costs in both regimes of interest, and belonged to primarily 3 resting-state networks, the DMN, frontoparietal control, and visual peripheral network, i.e., a combination of developing (DMN and control) and developed (visual peripheral) networks.

3.1.1. Effects of connectivity matrix thresholding on control cost estimates

Secondary analyses examined critical feedback costs estimated from adjacency matrices that had been obtained with a less conservative threshold (the 75th percentile of cross-correlation values). Results are summarized in Figures S3–S5 (heat maps for costs as a function of participant (S3) and region (S4), and spatial distribution of these costs (S5)). There was substantial spatial overlap of high critical control costs with those estimated using a more conservative threshold, although cost values were overall higher with the less conservative threshold. Median cosine similarity between critical costs estimated based on the two thresholds was high across assessments (>0.87). Similarly, at both assessments, the spatial distributions of high control costs (top 25 % and top 10 %) was also consistently high (BU ≥0.84). These findings suggest overall robustness of the results to thresholding.

3.1.2. Effects of fMRI run on control costs estimates

To assess the robustness of the results, the analyses were repeated using the second best-quality run, and estimated control costs were compared. At both assessments, cosine similarity of control costs in both regimes was moderate (0.5–0.67), and similarity between statistical model-predicted control costs (i.e., following adjustments for the percent of frames censored for motion, to account for potential

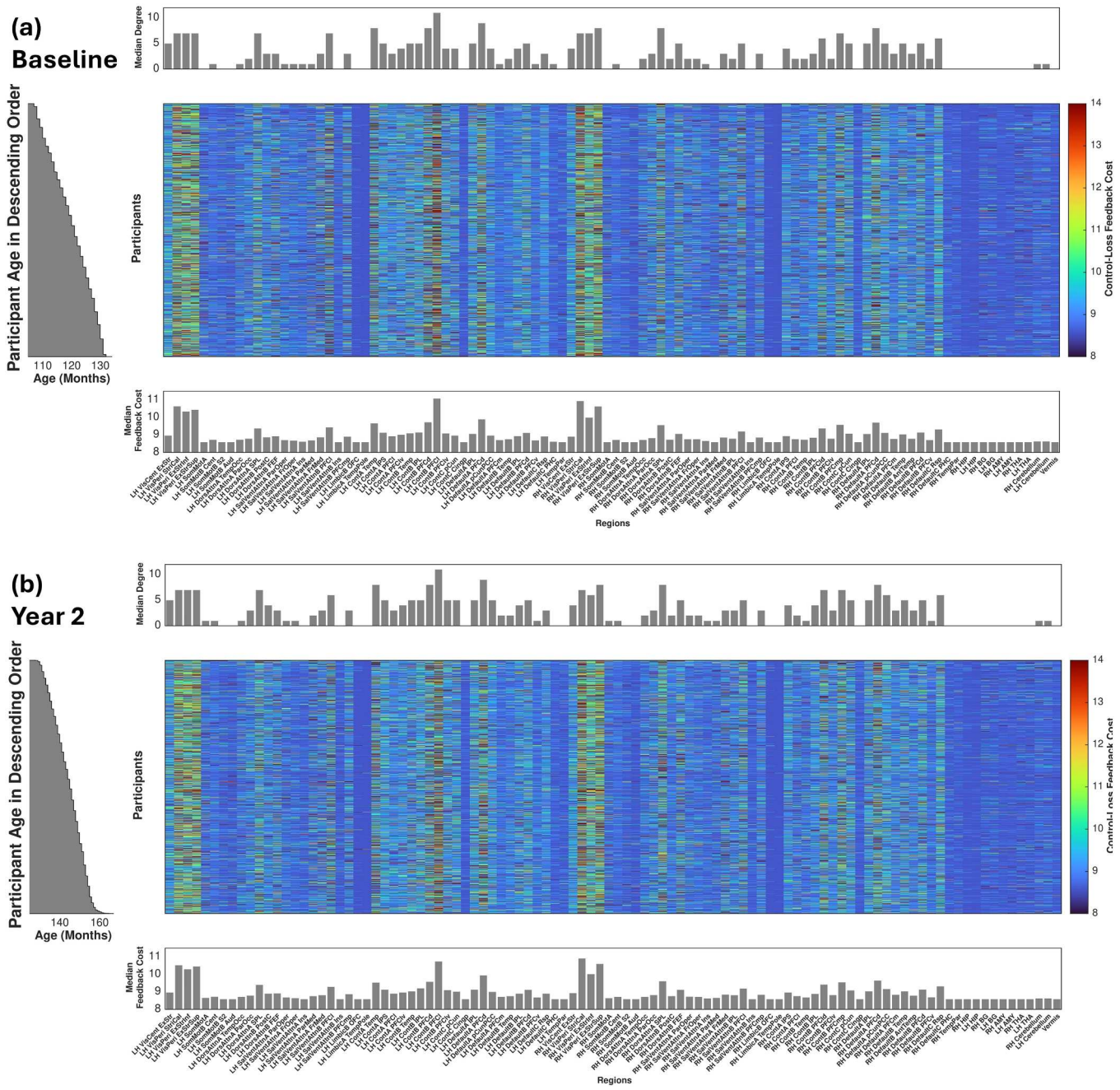

Fig. 1. Feedback costs at which regions lose their control action on the network, as a function of participants (y-axis) and analyzed regions (x-axis). The color range corresponds to cost values, estimated from the best-quality run at baseline (a) and two-year follow up (b). Participants are sorted by age. Median (over participants) node degree for each analyzed region is shown in the bar plot above each heat map, and median feedback costs in the bar plot below each heat map. All parameters were estimated using adjacency matrices obtained by thresholding corresponding connectivity matrices, based on the moderate outlying peak cross-correlation value.

differences in network density between runs) was high (>0.85). These results suggest statistical similarity of spatial control cost distributions estimated from distinct rs-fMRI runs.

3.1.3. *Effects of spatial resolution on control cost estimates*

To assess the impact of the spatial resolution at which the control costs were estimated, the analyses were repeated using a higher resolution parcellation (388 regions). Only the best-quality run was analyzed at this resolution. The spatial distribution of high critical costs and corresponding distribution of region degree at the two resolutions as shown in Fig. 3. Cosine similarity between critical cost estimates was moderate (median (IQR): 0.45 (0.18) at baseline, and 0.44 (0.19) at follow up). Similarity of spatial patterns of highest 25 % and 10 % costs was also moderate at both assessments (median (IQR) BU: 0.63 (0.15) - 0.67 (0.10)). These statistics suggest that control cost estimates may be sensitive to the spatial resolution of their assessment.

3.2. *Associations between feedback control costs and topological characteristics*

The distributions of regional connectedness, frequency of intrinsic activation (dynamic region engagement), net information flow and feedback costs at which regions lost their control action, at baseline (top) and two-year follow-up (bottom), are shown in Fig. 4. At both baseline and follow-up, similarity between the spatial distributions of degree and high control costs was high (median (IQR) BU: 0.91 (0.08) -

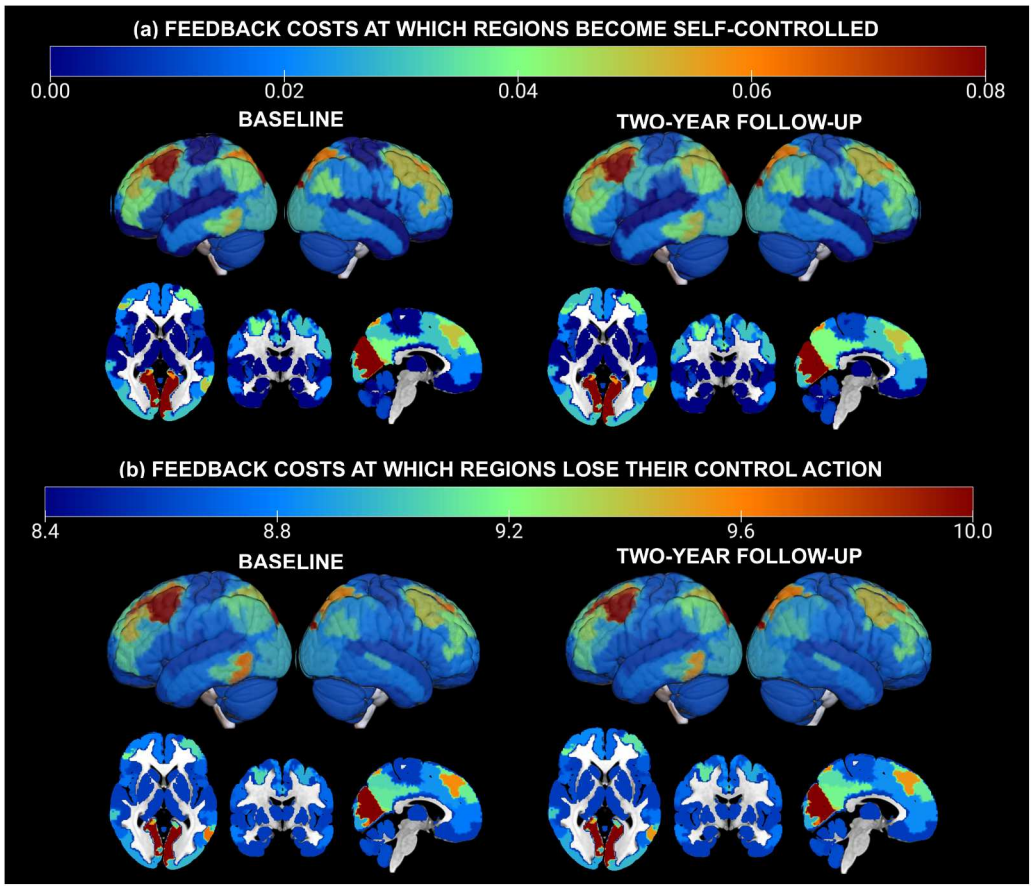

Fig. 2. Spatial distribution of median (across participants) feedback costs at which (a) a region's control action depends only on its own dynamic state, and (b) a region loses its control action over the network. Distributions are shown separately for baseline (left) and two-year follow up (right), and two-dimensional (horizontal, coronal, sagittal) slices and three-dimensional volumes are superimposed. Colors correspond to feedback cost values.

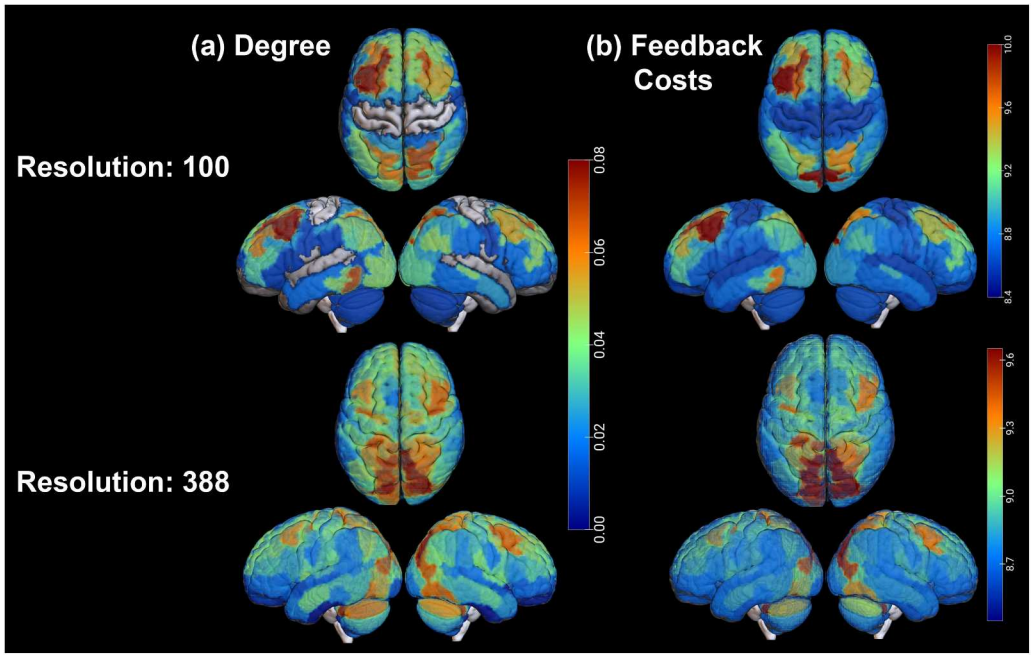

Fig. 3. Spatial distributions of feedback costs (right panels) and regional connectedness (left panels) estimated at two spatial resolutions (100 and 388 regions) at baseline. In left panels, color corresponds to median (across the sample) node degree, normalized to the maximum possible degree (99 and 387, respectively). In right panels it corresponds to feedback costs at which regions lose their control action over the network.

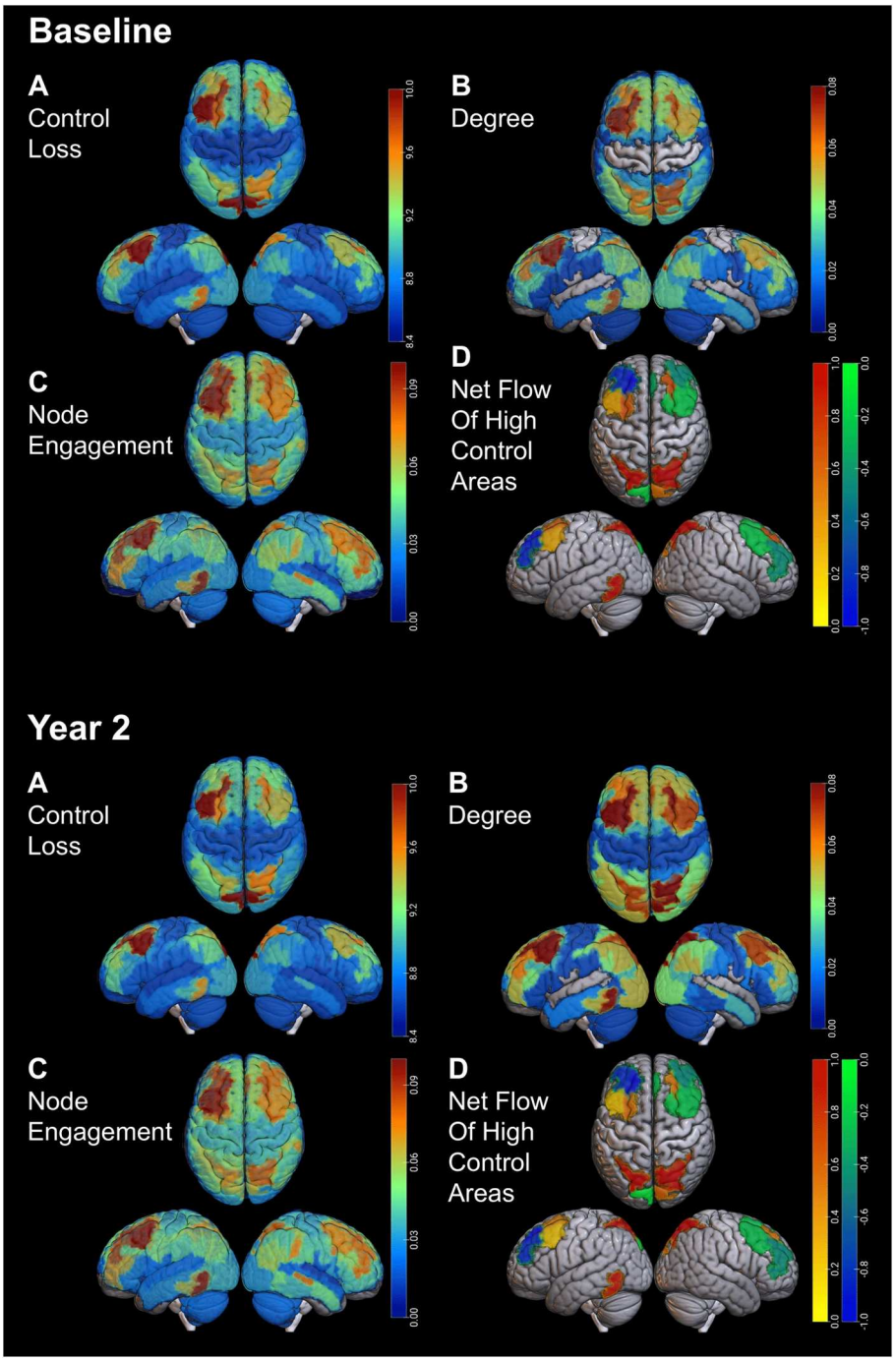

Fig. 4. Distribution of control costs and topological properties estimated from the baseline (top panels) and two-year follow-up (bottom panels) data. (A): feedback costs associated with a region losing their control action over the network; (B): local connectedness (degree); (C): Frequency of node engagement; (D): net information flow, (positive net flow indicates that the region receives more information than it outputs).

0.95 (0.05)), but moderate for dynamic region engagement (intrinsic regional activation) and control costs (median (IQR) BU: 0.59 (0.24) - 0.66 (0.16)). Ordinary linear regression models investigated associations between regions with top 25 % and 10 % critical feedback costs, respectively, and their topological properties.

A. Top 25 % of costs: Regions consistently associated with the top 25 % costs included posterior visual areas, bilateral prefrontal areas overlapping with frontoparietal control, salience and DM networks, bilateral parietal lobules overlapping with dorsal attention, control and default-mode networks, a left ventral posterior temporal area of the frontoparietal control network, and the right precuneus and retrosplenial cortex. Across assessments, degree was positively correlated with costs in all these regions, except for one area of the PFC (part of the DMN) at follow-up (baseline: $p < 0.01$, standardized regression coefficients (β) = 0.16 - 0.81, 95 % confidence interval (CI) = [0.11, 0.85]); follow up: $p < 0.01$, $\beta = 0.29$ - 0.82, 95 % CI = [0.23, 0.85]). Dynamic region engagement was positively correlated with feedback costs associated in most of these regions, both at baseline and follow up (baseline: $p < 0.04$, $\beta = 0.06$ to 0.24, 95 % CI = [0.01, 0.29]; follow up: $p < 0.01$, $\beta = 0.09$ - 0.24, 95 % CI = [0.04, 0.30]).

Across assessments, net information flow was negatively correlated with critical costs in multiple regions (i.e., regions associated with high

feedback costs receive and output similar amounts of information and thus net flow is lower), including bilateral visual areas, prefrontal cortical areas overlapping with salience, control and default-mode networks, left inferior temporal gyrus, right precuneus and right retrosplenial cortex ($p < 0.03$, $\beta = -0.33$ to -0.06, 95 % CI = [−0.38, −0.01]). At both assessments, net flow was positively associated with high feedback costs in the left ventral posterior temporal area ($p < 0.01$, $\beta = 0.29$, 95 % CI = [0.23, 0.34] at baseline, and $p < 0.01$, $\beta = 0.11$ to 0.26, 95 % CI = [0.05, 0.31] at follow up). Detailed associations and related model statistics are provided in Table 2.

B. Top 10 % of costs: Regions consistently associated with the top 10 % highest feedback costs included bilateral posterior visual areas, left prefrontal and temporal areas that are part of the frontoparietal control network, and a left dorsal prefrontal region that is part of the DMN (the right dorsal PFC was also associated with high control costs at follow up). At both baseline and follow up, degree was positively correlated with feedback costs in all of these regions, with the exception of the dorsal prefrontal area at follow-up (baseline: $p < 0.01$, $\beta = 0.16$ to 0.79, 95 % CI = [0.11, 0.82]; follow-up: $p < 0.01$, $\beta = 0.29$ to 0.78, 95 % CI = [0.23, 0.81]). Dynamic engagement was positively correlated with feedback cost in most regions, with the exception of the dorsal prefrontal area at baseline (baseline: $p < 0.01$, $\beta = 0.08$ to 0.18, 95 % CI = [0.03, 0.22]; follow-up: $p < 0.01$, $\beta = 0.14$ to 0.24, 95 % CI = [0.09 to 0.30]).

At baseline, net information flow was negatively correlated with feedback costs in the bilateral posterior visual areas ($p < 0.01$, $\beta = -0.20$ to -0.10, 95 % CI = [−0.25, −0.05]), and positively correlated in left ventral posterior temporal areas ($p < 0.01$, $\beta = 0.29$, 95 % CI = [0.23, 0.34]). At follow-up, net flow was negatively correlated with feedback costs in the same regions, including left dorsal PFC ($p < 0.01$, $\beta = -0.21$ to -0.12, 95 % CI = [−0.27, −0.07]), but positively correlated in left ventral posterior temporal areas ($p < 0.01$, $\beta = 0.26$, 95 % CI = [0.20, 0.31]). Detailed model statistics are provided in Table 2.

3.3. Pubertal changes in the distribution of feedback control costs

From baseline to follow-up, across regions age-related differences in critical feedback cost values were on average ≤1 %. Generalized linear mixed effects models that combined both baseline and follow-up samples, so that together they span the entire range of pubertal stages, were developed to examine changes in critical costs as a function of pubertal stage. Model statistics are summarized in Table 3. Consistently across runs, in most brain regions, puberty-related differences in critical feedback costs were nonsignificant. However, there was one exception. Based on data from the best (but not second) run, youth in later pubertal stages had higher feedback costs in the right cuneus ($p = 0.01$, $\beta = 0.07$, 95 % CI = [0.02, 0.13]).

3.4. Associations between feedback costs and participant characteristics

Consistently across fMRI runs, girls had higher costs associated with self-control in the right ventral temporal area ($p < 0.01$, $\beta = 0.01$, 95 % CI = [0.004, 0.016]) and lower costs in the left superior parietal lobule ($p < 0.04$, $\beta = -0.011$, 95 % CI = [−0.019, −0.003]). They also had higher costs associated with loss of control action in the bilateral inferior temporal gyrus and the hippocampus ($p < 0.05$, $\beta = 0.02$ to 0.63, 95 % CI = [0.001, 0.92]). They also had lower costs in the left superior parietal lobule and left postcentral gyrus ($p = 0.02$, $\beta = -0.53$ to -0.30, 95 % CI = [−0.89, −0.08]). BMI was associated with higher self-control costs in the right visual lingual gyrus and cuneus ($p < 0.03$, $\beta = [0.05, 0.06]$, 95 % CI = [0.01, 0.10]), and higher costs associated with loss of control action in the left superior temporal gyrus ($p < 0.02$, $\beta = 0.06$, 95 % CI = [0.02, 0.10]). There were no (consistent across runs) significant associations between critical control costs and race/ethnicity or family income. Model statistics are provided in Table 4. However, racial/ethnic minorities had lower critical control costs estimated from the best run in left prefrontal areas and the left inferior parietal cortex compared to the

Table 2
Statistics of ordinary linear regression models testing associations between control costs and topological characteristics. Reported p-values have been corrected for the False Discovery Rate.

PERCENTILE OF CONTROL COSTS	STATISTIC	SCANNING PERIOD	
		BASELINE	FOLLOW-UP
Topological Characteristic: Regional Connectedness (Degree)			
Top 25 %	Regions of positive correlations (+β)	Visual areas: Bilateral striate cortex; Bilateral cuneus; Bilateral lingual gyrus; Dorsal attention areas: Bilateral superior parietal lobule; Right frontal eye fields Salience areas: Bilateral lateral PFC Frontoparietal control areas: Bilateral PFC, including dorsolateral, ventrolateral & medial posterior; Left inferior parietal lobule; Left ventral posterior temporal cortex; Left inferior temporal gyrus Default-mode areas: Bilateral dorsal PFC; Right precuneus; Right retrosplenial cortex	Visual areas: Bilateral striate cortex; Bilateral cuneus; Bilateral lingual gyrus; Dorsal attention areas: Bilateral superior parietal lobule; Right frontal eye fields Salience areas: Bilateral lateral PFC Frontoparietal control areas: Bilateral PFC, including dorsolateral, ventrolateral & medial posterior; Right precuneus; Left inferior parietal lobule; Left ventral posterior temporal cortex; Default-mode areas: Bilateral dorsal PFC; Right precuneus; Right retrosplenial cortex; Left inferior parietal lobule
	Standardized β 95 % CI P-Value	[0.165, 0.814] [0.110, 0.8484] < 0.001	[0.287, 0.819] [0.234, 0.851] < 0.001
Top 10 %	Regions of positive correlations (+β)	Visual areas: Bilateral striate cortex; Bilateral cuneus; Bilateral lingual gyrus; Frontoparietal control areas: Left dorsal & lateral PFC Left ventral posterior temporal cortex; Default-mode areas: Left dorsal PFC	Visual areas: Bilateral striate cortex; Bilateral cuneus; Bilateral lingual gyrus; Frontoparietal control areas: Left lateral PFC Left ventral posterior temporal cortex; Default-mode areas: Right dorsal PFC
	Standardized β 95 % CI P-Value	[0.165, 0.789] [0.110, 0.823] < 0.001	[0.287, 0.775] [0.234, 0.811] < 0.001
Topological Characteristic: Regional Engagement			
Top 25 %	Regions of positive correlations (+β)	Visual areas: Bilateral striate cortex; Bilateral cuneus; Bilateral lingual gyrus; Dorsal attention areas: Left superior parietal lobule; Right frontal eye fields Salience areas:	Visual areas: Bilateral striate cortex; Bilateral cuneus; Bilateral lingual gyrus; Dorsal attention areas: Bilateral superior parietal lobule; Right frontal eye fields Salience areas:

(*continued on next page*)

Table 2 (*continued*)

PERCENTILE OF CONTROL COSTS	STATISTIC	SCANNING PERIOD	
		BASELINE	FOLLOW-UP
		Bilateral lateral PFC Frontoparietal control areas: Bilateral PFC, including dorsal, ventrolateral & medial posterior; Left inferior parietal lobule; Left ventral posterior temporal cortex; Default-mode areas: Bilateral dorsal PFC; Right precuneus; Right retrosplenial cortex	Bilateral lateral PFC Frontoparietal control areas: Bilateral PFC, including dorsolateral, ventrolateral & medial posterior; Right precuneus; Left inferior parietal lobule; Left ventral posterior temporal cortex; Default-mode areas: Bilateral dorsal PFC; Right precuneus; Right retrosplenial cortex; Left inferior parietal lobule
	Standardized β 95 % CI P-Value	[0.0579, 0.238] [0.003, 0.291] < 0.040	[0.093, 0.243] [0.038, 0.296] *P* < 0.001
Top 10 %	Regions of positive correlations (+β)	Visual areas: Bilateral striate cortex; Bilateral cuneus; Bilateral lingual gyrus; Frontoparietal control areas: Left dorsal and lateral PFC Left ventral posterior temporal cortex;	Visual areas: Bilateral striate cortex; Bilateral cuneus; Bilateral lingual gyrus; Frontoparietal control areas: Left lateral PFC; Left ventral posterior temporal cortex; Default-mode areas: Bilateral dorsal PFC
	Standardized β 95 % CI P-Value	[0.084, 0.178] [0.029, 0.232] < 0.003	[0.140, 0.243] [0.085, 0.296] < 0.001
Topological Characteristic: Net Information Flow			
Top 25 %	Regions of positive correlations (+β)	Frontoparietal control areas: Left ventral posterior temporal cortex;	Frontoparietal control areas: Left ventral posterior temporal cortex; Left dorsal PFC; Right precuneus
	Standardized β 95 % CI P-Value	0.286 [0.233, 0.339] < 0.001	[0.108, 0.257] [0.054, 0.310] < 0.002
	Regions of negative correlations (-β)	Visual areas: Bilateral striate cortex; Bilateral cuneus; Bilateral lingual gyrus; Salience areas: Bilateral lateral PFC Frontoparietal control areas: Right PFC, including dorsolateral & medial posterior; Left inferior temporal gyrus Default-mode areas: Bilateral dorsal PFC; Right precuneus; Right retrosplenial cortex	Visual areas: Bilateral striate cortex; Bilateral cuneus; Bilateral lingual gyrus; Salience areas: Bilateral lateral PFC Frontoparietal control areas: BilateralPFC, including ventrolateral, dorsolateral & medial posterior; Default-mode areas: Bilateral dorsal PFC; Left inferior parietal lobule; Right precuneus; Right retrosplenial cortex
	Standardized β 95 % CI P-Value	[−0.325, −0.064] [−0.377, −0.008] < 0.034	[−0.298, −0.073] [−0.352, −0.017] < 0.014
Top 10 %	Regions of positive correlations (+β)	Frontoparietal control areas: Left ventral posterior temporal cortex;	Frontoparietal control areas: Left ventral posterior temporal cortex;
	Standardized β 95 % CI P-Value	0.286 [0.233, 0.339] < 0.001	0.257 [0.204, 0.310] <0.001
	Regions of negative correlations (-β)	Visual areas: Bilateral striate cortex; Bilateral cuneus; Bilateral lingual gyrus;	Visual areas: Bilateral striate cortex; Bilateral cuneus; Bilateral lingual gyrus; Default-mode areas: Left dorsal PFC
	Standardized β 95 % CI P-Value	[−0.200, −0.102] [−0.255, −0.046] < 0.001	[−0.214, −0.121] [−0.270, −0.065] <0.001

Table 3
Statistics of mixed effects linear regression models testing associations between feedback costs at which regions lose their control action over the network and pubertal stage in individual regions, separately for each analyzed runs. Reported p-values have been corrected for the False Discovery Rate (FDR).

Associations Between Control Costs and Pubertal Stage		
Control Type	Statistic	Value
BEST-QUALITY RUN		
Cost at which regions lose control action over the network	Regions of positive correlations (+β) Standardized β* 95 % CI P-Value	Right cuneus 0.074 [0.015, 0.133] 0.041
SECOND-BEST-QUALITY RUN		
None		

rest of the cohort (which is predominantly white and non-Hispanic; $p < 0.04$, $\beta = -0.02$ to -0.17, 95 % CI = [−0.30, −0.04]). Model statistics are provided in Table S1.

4. Discussion

In a large sample of youth with early longitudinal data from the ABCD study, we have used a novel to Neuroscience, sparsity-promoting feedback control framework to investigate the controllability of developing brain circuits, assuming that their dynamics and topology depend on internal (latent) mechanisms. These mechanisms may represent a combination of biological/biochemical processes that are not directly measurable, but their action on the organization of the developing circuitry can be estimated. We selected this framework, which also assumes that the controller's action is sparse (i.e., a small number of regions with specific characteristics control the organization of the entire connectome), because it allowed us to incorporate the concepts of feedback penalty and sparsity, both critical to optimal network dynamics, and thus intrinsic and task-related synchronization of brain regions (Lizier et al., 2023).

The adolescent brain is not fully developed, and thus its circuitry is not yet topologically or dynamically optimal. Tracking the controllability of the adolescent connectome may provide important insights into its developmental optimization. Two critical ranges of feedback costs

Table 4
Statistics of mixed effects models testing associations between control costs and common demographics. Reported p-values have been corrected for the False Discovery Rate (FDR). Only statistics for regions that are repeated in both best and 2nd best run are reported.

Associations Between Control Costs and Demographics		
FEEDBACK COSTS AT WHICH REGIONS BECOME SELF-CONTROLLED		
Demographic	**Statistic**	**Value**
Sex	Regions of positive	Right middle temporal gyrus (part
(Boys = 1;	correlations (+β)	of the default-mode network)
Girls = 2)	β*	0.01
	95 % CI	[0.004, 0.016]
	P-Value	< 0.006
	Regions of negative	Left superior parietal lobule (part of
	correlations (-β)	dorsal attention network)
	β*	−0.011
	95 % CI	[−0.019, −0.003]
	P-Value	< 0.044
BMI Z-score	Regions of positive	Right visual lingual gyrus
(stratified by sex)	correlations (+β)	Right cuneus
	β*	[0.055, 0.056]
	95 % CI	[0.010, 0.101]
	P-Value	< 0.026
FEEDBACK COSTS AT WHICH REGIONS LOSE CONTROL ACTION		
Demographic	**Statistic**	**Value**
Sex	Regions of positive	Bilateral inferior temporal gyrus
	correlations (+β)	(part of control and default-mode
		network)
		Bilateral hippocampus;
	β*	[0.019, 0.629]
	95 % CI	[0.001, 0.917]
	P-Value	< 0.048
	Regions of negative	Left superior parietal lobule
	correlations (-β)	Left postcentral gyrus
	β*	[−0.531, −0.296]
	95 % CI	[−0.889, −0.075]
	P-Value	< 0.022
BMI Z-Score,	Regions of positive	Left superior temporal gyrus
(stratified by sex)	correlations (+β)	
	β*	0.059
	95 % CI	[0.015, 0.102]
	P-Value	< 0.016

were analyzed: a) costs at which the control action of individual regions only depends on themselves, and (typically high) costs at which regions lose their control action over the network. These costs were then examined as a function of regional topological properties, pubertal stage, and demographic characteristics.

In both regimes, high feedback costs were estimated in a small set of developed (primary visual) and developing (including prefrontal) regions. Higher costs were associated with higher regional connectedness and higher dynamic consistency, i.e., the region was consistently activated during spontaneous brain coordination at rest. Posterior areas associated with high feedback costs included regions that are part of the peripheral visual network and are well developed in adolescence, but also retrosplenial cortex, the cuneus and the superior parietal lobule (SPL), all of which continue to develop during adolescence as visual processing is refined, and also support other cognitive processes that evolve during this period (Vann et al., 2009; Miller et al., 2014; Wang et al., 2015; Mitchell et al., 2018; Palejwala et al., 2021). Other areas associated with high feedback costs were parts of the ventral temporal cortex (involved in visual recognition and categorization), which also continues to maturate in adolescence (Conway, 2018; Nordt et al., 2023). Together with the cuneus, SPL, and retrosplenial cortex, these areas are cognitive hubs, are involved in information integration and support multiple cognitive processes, including somatomotor processing, spatial navigation and shifting, memory, attentional control, but also posture and body part localization (Caminiti et al., 1996; Wopert et al., 1998; Wolbers et al., 2003; Makino et al., 2004; Felician et al., 2004; Molenberghs et al., 2007; Koenigs et al., 2009; Vandenberghe et al., 2011; Schmostein, 2012; Lester et al., 2014; Passarelli et al., 2021; Balcerek et al., 2021).

A number of regions associated with high feedback costs were in the prefrontal cortex, which undergoes accelerated maturation during adolescence, as high-level cognitive processes continue to develop (Nelson and Guyer, 2011; Somerville et al., 2013; Dumontheil, 2014; Caballero et al., 2016; Kolk and Rakic, 2022). These regions included dorsal and lateral prefrontal cortices, which support executive function and decision-making, memory and learning, and cognitive control (Wagner et al., 2001; Petrides, 2005 Fuster, 2015; Nee and D'Esposito, 2016), and are cognitive hubs as well (Gray et al., 2002; Milan et al., 2016; Menon and D'Esposito, 2022; Friedman and Robbins, 2022). Furthermore, together with the posterior areas associated with high feedback costs, they are part of a core set of brain regions that play a ubiquitous role in cognitive function (Dosenbach et al., 2006; Assem et al., 2020).

Most of the regions associated with high feedback costs have also been identified as topological hubs (i.e., highly connected and central to the organization of the connectome) that continue to evolve in adolescence (Tomasi and Volkow, 2011; Park and Friston, 2013; van der Heuvel and Sporns, 2013; Power et al., 2013; Hwang et al., 2013; Bertolero et al., 2015; Baker et al., 2015; Gordon et al., 2018; Oldham and Fornito, 2019). An independent ongoing investigation of these regions' topological characteristics in an overlapping sample has classified several of them as hubs that are stable during puberty. Higher feedback costs were associated with higher regional connectedness, suggesting that hubs maintain their control action over the connectome even at high costs. In addition, they were dynamically consistent, i.e., they were repeatedly highly connected during spontaneous synchronization of brain regions. These associations were also consistent across runs and assessments (following adjustments for differences in network density between runs and time of scan between assessments).

Finally, in most of these regions (with the exception of the ventral temporal cortex) higher feedback costs were associated with lower net information flow through them, i.e., with lower differences between information input and output from these regions. Brain hubs play a critical role in the communication between spatially distributed brain regions, by integrating information from them (e.g., resulting from domain-specific computations), and distributing the output of this synthesis in response to cognitive demands (van den Heuvel et al., 2012). Thus, information influx and outflux may be approximately equal in these regions, and thus net flow is low. The correlation between high feedback costs and low net flow again indicates that the identified regions may indeed be brain hubs, and suggests a positive association between controllability and communication cost.

Critical control costs were highly reproducible across thresholds, fMRI runs (and thus snapshots of brain activity) and assessments, i.e., from ages 9 - 12 years. Although the study examined a relatively narrow window of development (~3 years), in combination of the two assessments spanned the entire period of puberty. In most regions (with the exception of the right cuneus) these costs did not significantly change with pubertal stage, suggesting that their control action may be invariant to developmental changes at least during puberty, even if their local topology changes during this period. Indeed, many of these regions are elements of the DM and frontoparietal control networks, which are partly inter-connected (Dixon et al., 2018), and their topological organization and properties continue to develop significantly in adolescence (Fair et al., 2008; Sherman et al., 2014).

Despite its many strengths, including a novel to the field control framework, large early longitudinal sample that captured the heterogeneity of the developing adolescent brain, and cutting-edge analytic approaches for estimating topological/dynamic characteristics, the study had some limitations. Although the sample spanned the entire range of pubertal stages, it did not cover the entire adolescent period. To date, there are no other equally large samples covering this period. However, as the ABCD study continues to follow brain development in this cohort, additional longitudinal data will become available. Thus, a

future study could extend this investigation and track the brain's controllability, and the identified regions associated with high feedback costs, at later ages. However, within the period of this investigation, the identified invariance of control costs to age and pubertal stage is unlikely the result of ceiling effects, as the upper penalty limit used in calculations was much higher than the actual estimates. Furthermore, this study purposely focused only on the strongest connections of resting-state connectome, and estimated static and dynamic topological characteristics and information flow, directly from the fMRI time series. A few prior studies have examined the controllability of the structural connectome, but such an investigation was outside the scope of the present study. A future study could compare the controllability of structural and functional circuits in the same cohort, since the ABCD also collects diffusion MRI data. This study focused on brain regions with the strongest intrinsic connections at rest that were reproducible across snapshots (runs) of brain activity. It is, therefore, likely that they are well aligned with their anatomical constraints. In the case of a structural network, the control problem is solved in exactly the same way, assuming linear system dynamics. Thus, regions that were found to be critical to the controllability of the brain based on the strongest connections of the functional connectome likely overlap with regions that would be estimated from the structural connectome. Finally, the control problem was solved assuming linear system dynamics, which may be a simplification of potentially much more complex brain dynamics, especially in the developing brain. However, a recent study in adults, comparing linear and nonlinear models has shown that at the macroscale, human brain dynamics (encoded in electrophysiological and resting-state fMRI signals) are well described by linear models (Nozari et al., 2024), in part as a result of spatio-temporal averaging of microscopic brain dynamics, which are nonlinear. It is anticipated that at this scale, intrinsic dynamics of the adolescent brain are adequately described by a linear model, especially for the purpose of estimating control costs, but a future study could compare linear and nonlinear models in youth.

Despite a few limitations, this study makes a significant and novel contribution to the field by using a powerful modeling approach to a address the fundamental question of how network dynamics are controlled in the developing brain, which is suboptimally organized and changes significantly, especially in adolescence. To the best of our knowledge, this is the first large-scale application of this framework to developing brain networks. The study has identified a parsimonious set of highly reproducible (across snapshots of resting-state activity) and developmentally stable regions that exert their action on intrinsic brain network dynamics even at high feedback costs. Most of these regions are core cognitive hubs and highly connected functional hubs that are central to the organization of the connectome and cognitive function across domains. An important finding is that in contrast to topological characteristics that change as a function of age and neural maturation (even within a period of two years), the distribution of regions exerting their control action on the brain and the associated feedback costs do not, at least within the period of observation in this study. These results provide novel insights into an important yet relatively underexplored mechanism of brain network dynamics. They suggest that even the underdeveloped (and in some areas redundantly connected) adolescent brain, fundamental mechanisms of system controllability may be well developed, as reflected in the small set of distributed regions that exert their action on the connectome, to facilitate information processing and response to cognitive demands.

Funding statement

This study was supported by the National Science Foundation awards #1940094, 1649865, 2207733 (CS, JL), #2207699, 1938914 (IM, PD)

Ethics statement

This study involved secondary analyses of publicly available, de-identified human data and was approved by the Institutional Review Board.

Data/code availability statement

This study analyzed publicly available data from the ABCD study. All data are available through the National Institute of Mental Health Data Archive (NDA). https://nda.nih.gov/.

All codes associated with this study have been made publicly available:

Codes associated with the fMRI data analyses can be found at: https://github.com/cstamoulis1/Next-Generation-Neural-Data-Analysis-NGNDA-

Codes associated with statistical analyses in this manuscript can be found at: https://github.com/cstamoulis1/Closed-Loop-Control-of-Developing-Brain-Networks/.

CRediT authorship contribution statement

Jethro Lim: Writing – review & editing, Writing – original draft, Visualization, Validation, Software, Formal analysis. **Ilias Mitrai:** Writing – review & editing, Writing – original draft, Visualization, Software, Methodology, Formal analysis. **Prodromos Daoutidis:** Writing – review & editing, Writing – original draft, Supervision, Methodology, Investigation, Funding acquisition, Conceptualization. **Catherine Stamoulis:** Writing – review & editing, Writing – original draft, Validation, Supervision, Software, Resources, Project administration, Methodology, Investigation, Funding acquisition, Conceptualization.

Declaration of competing interest

None of the authors have any competing interests.

Supplementary materials

Supplementary material associated with this article can be found, in the online version, at doi:10.1016/j.neuroimage.2025.121562.

References

Assaf, M., Jagannathan, K., Calhoun, V.D., et al., 2010. Abnormal functional connectivity of default mode sub-networks in autism spectrum disorder patients. Neuroimage 53, 247–256.

Assem, M., Glasser, M.F., Van Essen, D.C., Duncan, J., 2020. A domain-general cognitive core defined in multimodally parcellated human cortex. Cerebral Cortex 30 (8), 4361–4380.

Baker, S.T., Lubman, D.I., Yücel, M., Allen, N.B., Whittle, S., Fulcher, B.D., Fornito, A., 2015. Developmental changes in brain network hub connectivity in late adolescence. J. Neurosci. 35 (24), 9078–9087.

Balcerek, E., Włodkowska, U., Czajkowski, R., 2021. Retrosplenial cortex in spatial memory: focus on immediate early genes mapping. Mol. Brain 14, 172.

Bassett, D.S., Bullmore, E.T., 2017. Small-world brain networks revisited. Neuroscientist. 23 (5), 499–516. Oct.

Benjamini, Y, Hochberg, Y, 1995. Controlling the false discovery rate: a practical and powerful approach to multiple testing. J Royal Stat Soc, Series B 57 (1), 289–300.

Bertolero, M.A., Yeo, B.T.T., D'Esposito, M., 2015. The modular and integrative functional architecture of the human brain. Proc. Natl. Acad. Sci. 112 (49). https://doi.org/10.1073/pnas.1510619112.

Betzel, R.F., Gu, S., Medaglia, J.D., Pasqualetti, F., Bassett, D.S., 2016. Optimally controlling the human connectome: the role of network topology. Sci. Rep. 6, 30770. https://doi.org/10.1038/srep30770.

Boyd, S., Parikh, N., Chu, E., Peleato, B., Eckstein, J., 2011. Distributed optimization and statistical learning via the alternating direction method of multipliers. Now Found. Trends. https://doi.org/10.1561/2200000016.

Braun, U., Harneit, A., Pergola, G., Menara, T., Schäfer, A., Betzel, R.F., Zang, Z., Schweiger, J.I., Zhang, X., Schwarz, K., Chen, J., Blasi, G., Bertolino, A., Durstewitz, D., Pasqualetti, F., Schwarz, E., Meyer-Lindenberg, A., Bassett, D.S., Tost, H., 2021. Brain network dynamics during working memory are modulated by

dopamine and diminished in schizophrenia. Nat. Commun. 12 (1), 3478. https://doi.org/10.1038/s41467-021-23694-9.
Breakspear, M., 2017. Dynamic models of large-scale brain activity. Nat. Neurosci. 20 (3), 340–352.
Brooks, S.J., Parks, S.M., Stamoulis, C., 2021. Widespread positive direct and indirect effects of regular physical activity on the developing functional connectome in early adolescence. Cerebral Cortex 31 (10), 4840–4852. https://doi.org/10.1093/cercor/bhab126. PMID: 33987673.
Caballero, A., Granberg, R., Tseng, K.Y., 2016. Mechanisms contributing to prefrontal cortex maturation during adolescence. Neurosci. Biobehav. Rev. 70, 4–12.
Caminiti, R., Ferraina, S., Johnson, P.B., 1996. The sources of visual information to the primate frontal lobe: a novel role for the superior parietal lobule. Cerebral Cortex 6 (3), 319–328.
Casey, BJ, Cannonier, T, Conley, MI, 2018. ABCD Imaging Acquisition Workgroup. 2018. The Adolescent Brain Cognitive Development (ABCD) study: Imaging acquisition across 21 sites. Developmental Cognitive Neuroscience 3 (2), 43–54.
Chén, O.Y., Cao, H., Reinen, J.M., Qian, T., Gou, J., Phan, H., De Vos, M., Cannon, T.D., 2019. Resting-state brain information flow predicts cognitive flexibility in humans. Sci. Rep. 9 (1), 3879. Mar 7.
Chase, H.W., Phillips, M.L., 2016. Elucidating neural network functional connectivity abnormalities in bipolar disorder: toward a harmonized methodological approach. Biol. Psychiatry: Cogn. Neurosci. Neuroimaging 1, 288–298.
Cherkassky Vladimir, L., Kana Rajesh, K., Keller Timothy, A., Just Marcel, Adam, 2006. Functional connectivity in a baseline resting-state network in autism. Neuroreport 17, 1687–1690.
Cocchi, L., Zalesky, A., Fornito, A., Mattingley, J.B., 2013. Dynamic cooperation and competition between brain systems during cognitive control. Trends Cogn. Sci. (Regul. Ed.) 17 (10), 493–501. https://doi.org/10.1016/j.tics.2013.08.006.
Constantino, P.H., Tang, W., Daoutidis, P., 2019. Topology effects on sparse control of complex networks with laplacian dynamics. Sci. Rep. 9 (1), 9034. https://doi.org/10.1038/s41598-019-45476-6.
Conway, B.R., 2018. The organization and operation of inferior temporal cortex. Annu. Rev. Vis. Sci. 15 (4), 381–402.
Cui, Z., Stiso, J., Baum, G.L., Kim, J.Z., Roalf, D.R., Betzel, R.F., Gu, S., Lu, Z., Xia, C.H., He, X., Ciric, R., Oathes, D.J., Moore, T.M., Shinohara, R.T., Ruparel, K., Davatzikos, C., Pasqualetti, F., Gur, R.E., Gur, R.C., Bassett, D.S., Satterthwaite, T.D., 2020. Optimization of energy state transition trajectory supports the development of executive function during youth. Elife 9, e53060. https://doi.org/10.7554/eLife.53060.
Deco, G., Jirsa, V.K., McIntosh, A.R., 2011. Emerging concepts for the dynamical organization of resting-state activity in the brain. Nat. Rev. Neurosci. 12 (1), 43–56. Jan.
Deng, S., Li, J., Thomas Yeo, B.T., Gu, S., 2022. Control theory illustrates the energy efficiency in the dynamic reconfiguration of functional connectivity. Commun. Biol. 5 (1), 295. https://doi.org/10.1038/s42003-022-03196-0.
Diedrichsen J, Balsters JH, Flavell J, et al. 2009. A probabilistic MR atlas of the human cerebellum, NeuroImage, 46 (1): 39-46.
Dixon, M.L., De, La, Vega, A., Mills, C., Andrews-Hanna, J., Spreng, R.N., Cole, M.W., Christoff, K., 2018. Heterogeneity within the frontoparietal control network and its relationship to the default and dorsal attention networks. Proc. Natl. Acad. Sci. 115 (7), E1598–E1607.
Dosenbach, N.U., Visscher, K.M., Palmer, E.D., Miezin, F.M., Wenger, K.K., Kang, H.C., Petersen, S.E., 2006. A core system for the implementation of task sets. Neuron 50 (5), 799–812.
Dumontheil, I., 2014. Development of abstract thinking during childhood and adolescence: the role of rostrolateral prefrontal cortex. Dev. Cogn. Neurosci. 10, 57–76.
Eavani, H., Satterthwaite, T.D., Filipovych, R., Gur, R.E., Gur, R.C., Davatzikos, C., 2015. Identifying sparse connectivity patterns in the brain using resting-state fMRI. Neuroimage 105, 286–299. Jan 15.
Fair, D.A., Cohen, A.L., Dosenbach, N.U., Church, J.A., Miezin, F.M., Barch, D.M., Schlaggar, B.L., 2008. The maturing architecture of the brain's default network. Proc. Natl. Acad. Sci. 105 (10), 4028–4032.
Felician, O., Romaiguère, P., Anton, J.L., Nazarian, B., Roth, M., Pot, M., Roll, J.P., 2004. The role of human left superior parietal lobule in body part localization. Ann. Neurol.: Off. J. Am. Neurol. Assoc. Child Neurol. Soc. 55 (5), 749–751.
Friedman, N.P., Robbins, T.W., 2022. The role of prefrontal cortex in cognitive control and executive function. Neuropsychopharmacology 47 (1), 72–89.
Fuster, J., 2015. The Prefrontal Cortex. Academic press.
Geweke, J., 1982. Measurement of linear-dependence and feedback between multiple time-series. J. Am. Stat. Assoc. 77, 304–313.
Gordon, E.M., Lynch, C.J., Gratton, C., Laumann, T.O., Gilmore, A.W., Greene, D.J., Nelson, S.M., 2018. Three distinct sets of connector hubs integrate human brain function. Cell Rep. 24 (7), 1687–1695.
Gray, J.R., Braver, T.S., Raichle, M.E., 2002. Integration of emotion and cognition in the lateral prefrontal cortex. Proc. Natl. Acad. Sci. 99 (6), 4115–4120.
Gu, S., Pasqualetti, F., Cieslak, M., Telesford, Q.K., Yu, A.B., Kahn, A.E., Medaglia, J.D., Vettel, J.M., Miller, M.B., Grafton, S.T., Bassett, D.S., 2015. Controllability of structural brain networks. Nat. Commun. 6, 8414. https://doi.org/10.1038/ncomms9414.
Gu, S., Betzel, R.F., Mattar, M.G., Cieslak, M., Delio, P.R., Grafton, S.T., Pasqualetti, F., Bassett, D.S., 2017. Optimal trajectories of brain state transitions. Neuroimage 148, 305–317. https://doi.org/10.1016/j.neuroimage.2017.01.003.
Hagler Jr, D.J., Hatton, S., Cornejo, M.D., Makowski, C., Fair, D.A., Dick, A.S., Sutherland, M.T., Casey, B.J., Barch, D.M., Harms, M.P., Watts, R., Bjork, J.M., Garavan, H.P., Hilmer, L., Pung, C.J., Sicat, C.S., Kuperman, J., Bartsch, H., Xue, F., Heitzeg, M.M., Dale, A.M., 2019. Image processing and analysis methods for the adolescent brain cognitive development study. Neuroimage 202, 116091. https://doi.org/10.1016/j.neuroimage.2019.116091.
Hansen, E.C., Battaglia, D., Spiegler, A., Deco, G., Jirsa, V.K., 2015. Functional connectivity dynamics: modeling the switching behavior of the resting state. Neuroimage 105, 525–535. https://doi.org/10.1016/j.neuroimage.2014.11.001. Jan 15.
Hu, L., Katz, E.S., Stamoulis, C., 2023. Modulatory effects of fMRI acquisition time of day, week and year on adolescent functional connectomes across spatial scales: implications for inference. Neuroimage 284, 120459. Dec 15.
Hwang, K., Hallquist, M.N., Luna, B., 2013. The development of hub architecture in the human functional brain network. Cerebral Cortex 23 (10), 2380–2393.
Koenigs, M., Barbey, A.K., Postle, B.R., Grafman, J., 2009. Superior parietal cortex is critical for the manipulation of information in working memory. J. Neurosci. 29 (47), 14980–14986.
Kolk, S.M., Rakic, P., 2022. Development of prefrontal cortex. Neuropsychopharmacology 47 (1), 41–57.
Konrad, K., Eickhoff, S.B., 2010. Is the ADHD brain wired differently? A review on structural and functional connectivity in attention deficit hyperactivity disorder. Hum. Brain Mapp. 31, 904–916.
Kottaram, A., Johnston, L.A., Cocchi, L., Ganella, E.P., Everall, I., Pantelis, C., Kotagiri, R., Zalesky, A., 2019. Brain network dynamics in schizophrenia: reduced dynamism of the default mode network. Hum. Brain Mapp. 40 (7), 2212–2228. May.
Kringlebach, M.L., Deco, G., 2020. Brain States and transitions: insights from computational neuroscience. Cell Rep. 32 (10), 108128.
Lee, B., Kang, U., Chang, H., Cho, K.H, 2019. The hidden control architecture of complex brain networks. iScience 13, 154–162.
Lester, B.D., Dassonville, P., 2014. The role of the right superior parietal lobule in processing visual context for the establishment of the egocentric reference frame. J. Cogn. Neurosci. 26 (10), 2201–2209.
Lim, J, Mitrai, I, Daoutidis, P, Stamoulis, C, 2024. Effects of topology on the controllability of brain connectomes through sparsity promoting control. Annu Int Conf IEEE Eng Med Biol Soc 1-4.
Lim, J., Cooper, K., Stamoulis, C., 2025. Dynamic fluctuations of resting-state topology and signal amplitude are biomarkers of brain development in adolescence. Network Neuroscience 9 (3), 1039–1064.
Lin, F., Fardad, M., Jovanovic, M., 2013. Design of optimal sparse feedback gains via the alternating direction method of multipliers. IEEE Trans. Autom. Control 58 (9), 2426–2431. https://doi.org/10.1109/TAC.2013.2257618.
Lizier, J.T., Bauer, F., Atay, F.M., Jost, J., 2023. Analytic relationship of relative synchronizability to network structure and motifs. Proc. Natl. Acad. Sci. 120 (37), e2303332120.
Lobier, M., Siebenhühner, F., Palva, S., Palva, J.M., 2013. Phase Transfer entropy: a novel phase-based measure for directed connectivity in networks coupled by oscillatory interactions. Neuroimage 85. https://doi.org/10.1016/j.neuroimage.2013.08.0.
Makino, Y., Yokosawa, K., Takeda, Y., Kumada, T., 2004. Visual search and memory search engage extensive overlapping cerebral cortices: an fMRI study. Neuroimage 23 (2), 525–533.
Menon, V., D'Esposito, M., 2022. The role of PFC networks in cognitive control and executive function. Neuropsychopharmacology 47 (1), 90–103. Jan.
Meyer-Lindenberg, A., Ziemann, U., Hajak, G., Cohen, L., Berman, K.F., 2002. Transitions between dynamical states of differing stability in the human brain. Proc. Natl. Acad. Sci. U S. A 99 (17), 10948–10953. https://doi.org/10.1073/pnas.162114799.
Millan, M.J., Rivet, J.M., Gobert, A., 2016. The frontal cortex as a network hub controlling mood and cognition: probing its neurochemical substrates for improved therapy of psychiatric and neurological disorders. J. Psychopharmacol. 30 (11), 1099–1128.
Miller, A.M., Vedder, L.C., Law, L.M., Smith, D.M., 2014. Cues, context, and long-term memory: the role of the retrosplenial cortex in spatial cognition. Front. Hum. Neurosci. 8, 586, 2014.
Mitchell, A.S., Czajkowski, R., Zhang, N., Jeffery, K., Nelson, A.J.D., 2018. Retrosplenial cortex and its role in spatial cognition. Brain Neurosci. Adv. 2, 2398212818757098.
Mitrai, I., Stamoulis, C., Daoutidis, P., 2021. A sparse H∞ controller synthesis perspective on the reconfiguration of brain networks. In: Proceedings of the American Control Conference (ACC), pp. 1204–1209. https://doi.org/10.23919/ACC50511.2021.9483169.
Mitrai, I., Jones, V.O., Dewantoro, H., Stamoulis, C., Daoutidis, P., 2023. Internal control of brain networks via sparse feedback. AIChE J. 69 (4). https://doi.org/10.1002/aic.18061.
Molenberghs, P., Mesulam, M.M., Peeters, R., Vandenberghe, R.R., 2007. Remapping attentional priorities: differential contribution of superior parietal lobule and intraparietal sulcus. Cerebral Cortex 17 (11), 2703–2712.
Nee, D.E., D'Esposito, M., 2016. The hierarchical organization of the lateral prefrontal cortex. Elife 5, e12112.
Nelson, E.E., Guyer, A.E., 2011. The development of the ventral prefrontal cortex and social flexibility. Dev. Cogn. Neurosci. 1 (3), 233–245.
Nordt, M., Gomez, J., Natu, V.S., Rezai, A.A., Finzi, D., Kullar, A., Grill-Spector, K., 2023. Longitudinal development of category representations in ventral temporal cortex predicts word and face recognition. Nat. Commun. 14, 8010, 2023.
Nozari, E., Bertolero, M.A., Stiso, J., Caciagli, L., Cornblath, E.J., He, X., Mahadevan, A. S., Pappas, G.J., Bassett, D.S., 2024. Macroscopic resting-state brain dynamics are best described by linear models. Nat. Biomed. Eng. 8 (1), 68–84. Jan.
Oldham, S., Fornito, A., 2019. The development of brain network hubs. Dev. Cogn. Neurosci. 36, 100607.

Palejwala, A.H., Dadario, N.B., Young, I.M., O'Connor, K., Briggs, R.G., Conner, A.K., O'Donoghue, D.L., Sughrue, M.E., 2021. Anatomy and white matter connections of the lingual gyrus and cuneus. World Neurosurg. 151, e426–e437.
Park, H.J., Friston, K., 2013. Structural and functional brain networks: from connections to cognition. Science (1979) 342 (6158), 1238411.
Parkes, L., Moore, T.M., Calkins, M.E., Cieslak, M., Roalf, D.R., Wolf, D.H., Gur, R.C., Gur, R.E., Satterthwaite, T.D., Bassett, D.S., 2021. Network controllability in transmodal cortex predicts positive psychosis spectrum symptoms. Biol. Psychiatry 90 (6), 409–418. https://doi.org/10.1016/j.biopsych.2021.03.016.
Parkes, L., Kim, J.Z., Stiso, J., Brynildsen, J.K., Cieslak, M., Covitz, S., Gur, R.E., Gur, R. C., Pasqualetti, F., Shinohara, R.T., Zhou, D., Satterthwaite, T.D., & Bassett, D.S. (2023). Using network control theory to study the dynamics of the structural connectome. bioRxiv., 2023.08.23.554519. 10.1101/2023.08.23.554519.
Pasqualetti, F., Zampieri, S., Bullo, F., 2014. Controllability metrics, limitations and algorithms for complex networks. IEEE Trans. Control Netw. Syst. 1 (1), 40–52. https://doi.org/10.1109/TCNS.2014.2310254.
Passarelli, L., Gamberini, M., Fattori, P., 2021. The superior parietal lobule of primates: a sensory-motor hub for interaction with the environment. J. Integr. Neurosci. 20 (1), 157–171.
Petersen, A.C., Crockett, L., Richards, M., Boxer, A., 1988. A self-report measure of pubertal status: reliability, validity, and initial norms. J. Youth. Adolesc. 17 (2), 117–133. https://doi.org/10.1007/BF01537962. Apr.
Petrides, M., 2005. Lateral prefrontal cortex: architectonic and functional organization. Philos Trans R Soc Lond B Biol Sci 360 (1456), 781–795.
Power, J.D., Schlaggar, B.L., Lessov-Schlaggar, C.N., Petersen, S.E., 2013. Evidence for hubs in human functional brain networks. Neuron 79 (4), 798–813.
Schaefer, A, Kong, R, Gordon, EM, Laumann, TO, Zuo, XN, Holmes, AJ, Eickhoff, SB, Yeo, BTT, 2018. Local-Global Parcellation of the Human Cerebral Cortex from Intrinsic Functional Connectivity MRI. Cereb Cortex, 28((9)), 3095–3114.
Sherman, L.E., Rudie, J.D., Pfeifer, J.H., Masten, C.L., McNealy, K., Dapretto, M., 2014. Development of the default mode and central executive networks across early adolescence: a longitudinal study. Dev. Cogn. Neurosci. 10, 148–159.
Shine, J.M., Poldrack, R.A., 2018. Principles of dynamic network reconfiguration across diverse brain states. Neuroimage 180, 396–405.
Shomstein, S., 2012. Cognitive functions of the posterior parietal cortex: top-down and bottom-up attentional control. Front. Integr. Neurosci. 6, 38.
Sitaram, R., Ros, T., Stoeckel, L., Haller, S., Scharnowski, F., Lewis-Peacock, J., Weiskopf, N., Blefari, M.L., Rana, M., Oblak, E., Birbaumer, N., Sulzer, J., 2017. Closed-loop brain training: the science of neurofeedback. Nat. Rev. Neurosci. 18 (2), 86–100. https://doi.org/10.1038/nrn.2016.164.
Somerville, L.H., Jones, R.M., Ruberry, E.J., Dyke, J.P., Glover, G., Casey, B.J., 2013. The medial prefrontal cortex and the emergence of self-conscious emotion in adolescence. Psychol. Sci. 24 (8), 1554–1562.
Taghia, J., Cai, W., Ryali, S., Kochalka, J., Nicholas, J., Chen, T., Menon, V., 2018. Uncovering hidden brain state dynamics that regulate performance and decision-making during cognition. Nat. Commun. 9 (1), 2505.
Tian Y, Margulies DS, Breakspear M, et al. 2020.Topographic organization of the human subcortex unveiled with functional connectivity gradients. Nat Neurosc, 23 (11): 1421-1432.
Tognoli, E., Kelso, J.S., 2014. The metastable brain. Neuron, 81 (1), 35–48.
Tomasi, D., Volkow, N.D., 2011. Association between functional connectivity hubs and brain networks. Cerebral cortex 21 (9), 2003–2013.
Van den Heuvel, M.P., Fornito, A., 2014. Brain networks in schizophrenia. Neuropsychol. Rev. 24 (1), 32–48. Mar.
Van den Heuvel, M.P., Sporns, O., 2011. Rich-club organization of the human connectome. J. Neurosci. 31 (44), 15775–15786. https://doi.org/10.1523/JNEUROSCI.3539-11.2011.
Van den Heuvel, M.P., Sporns, O., 2013. Network hubs in the human brain. Trends Cogn. Sci. (Regul. Ed.) 17 (12), 683–696.
Van den Heuvel, M.P., Kahn, R.S., Goñi, J., Sporns, O., 2012. High-cost, high-capacity backbone for global brain communication. Proc. Natl. Acad. Sci. U. S. A. 109 (28), 11372–11377. Jul 10.
Vann, S.D., Aggleton, J.P., Maguire, E.A., 2009. What does the retrosplenial cortex do? Nat. Rev. Neurosci. 10 (11), 792–802.
Vidaurre, D., Smith, S.M., Woolrich, M.W., 2017. Brain network dynamics are hierarchically organized in time. Proc. Natl. Acad. Sci. 114 (48), 12827–12832.
Wagner, A.D., Maril, A., Bjork, R.A., Schacter, D.L., 2001. Prefrontal contributions to executive control: fMRI evidence for functional distinctions within lateral prefrontal cortex. Neuroimage 14 (6), 1337–1347.
Wang, J., Yang, Y., Fan, L., Xu, J., Li, C., Liu, Y., Jiang, T., 2015. Convergent functional architecture of the superior parietal lobule unraveled with multimodal neuroimaging approaches. Hum. Brain Mapp. 36 (1), 238–257.
Wilmskoetter, J., He, X., Caciagli, L., Jensen, J.H., Marebwa, B., Davis, K.A., Fridriksson, J., Basilakos, A., Johnson, L.P., Rorden, C., Bassett, D., Bonilha, L., 2022. Language recovery after brain injury: a structural network control theory study. J. Neurosci. 42 (4), 657–669. https://doi.org/10.1523/JNEUROSCI.1096-21.2021.
Wolbers, T., Weiller, C., Büchel, C., 2003. Contralateral coding of imagined body parts in the superior parietal lobe. Cerebral cortex 13 (4), 392–399.
Wolpert, D.M., Goodbody, S.J., Husain, M., 1998. Maintaining internal representations: the role of the human superior parietal lobe. Nat. Neurosci. 1 (6), 529–533.
Wright, J., Macefield, V.G., van Schaik, A., Tapson, J.C., 2016. A review of control strategies in closed-loop neuroprosthetic systems. Front. Neurosci. 10, 312. https://doi.org/10.3389/fnins.2016.00312.
Yeo, BT, Krienen, FM, Sepulcre, J, Sabuncu, MR, Lashkari, D, Hollinshead, M, Roffman, JL, Smoller, JW, Zöllei, L, Polimeni, JR, Fischl, B, Liu, H, Buckner, RL, 2011. The organization of the human cerebral cortex estimated by intrinsic functional connectivity. J Neurophysiol 106 (3), 1125–1165.
Zöller, D., Sandini, C., Schaer, M., Eliez, S., Bassett, D.S., Van De Ville, D., 2021. Structural control energy of resting-state functional brain states reveals less cost-effective brain dynamics in psychosis vulnerability. Hum. Brain Mapp. 42 (7), 2181–2200. https://doi.org/10.1002/hbm.25358.
Zhang, Q., Hu, S., Talay, R., Xiao, Z., Rosenberg, D., Liu, Y., Sun, G., Li, A., Caravan, B., Singh, A., Gould, J.D., Chen, Z.S., Wang, J., 2023. A prototype closed-loop brain-machine interface for the study and treatment of pain. Nat. Biomed. Eng. 7 (4), 533–545. https://doi.org/10.1038/s41551-021-00736-7.
Zrenner, C., Belardinelli, P., Müller-Dahlhaus, F., Ziemann, U., 2016. Closed-loop neuroscience and non-invasive brain stimulation: a tale of two loops. Front. Cell Neurosci. 10, 92. https://doi.org/10.3389/fncel.2016.00092.

Further reading

Bookheimer, S.Y., Salat, D.H., Terpstra, M., Ances, B.M., Barch, D.M., Buckner, R.L., Burgess, G.C., Curtiss, S.W., Diaz-Santos, M., Elam, J.S., Fischl, B., Greve, D.N., Hagy, H.A., Harms, M.P., Hatch, O.M., Hedden, T., Hodge, C., Japardi, K.C., Kuhn, T. P., Ly, T.K., Smith, S.M., Somerville, L.H., Uğurbil, K., van der Kouwe, A., Van Essen, D., Woods, R.P., Yacoub, E., 2019. The lifespan human connectome project in aging: an overview. Neuroimage 185, 335–348 Jan 15.
Bullmore, E., Sporns, O., 2012. The economy of brain network organization. Nat. Rev. Neurosci. 13 (5), 336–349. https://doi.org/10.1038/nrn3214.
Di, X., Xu, T., Uddin, L.Q., Biswal, B.B., 2023. Individual differences in time-varying and stationary brain connectivity during movie watching from childhood to early adulthood: age, sex, and behavioral associations. Dev. Cogn. Neurosci. 63, 101280. https://doi.org/10.1016/j.dcn.2023.101280.
Fu, Z., Sui, J., Iraji, A., Liu, J., Calhoun, V.D., 2024. Cognitive and psychiatric relevance of dynamic functional connectivity states in a large (N > 10,000) children population. Mol. Psychiatry Advance online publication. https://doi.org/10.1038/s41380-024-02683-6.
Mahadevan, A.S., Cornblath, E.J., Lydon-Staley, D.M., Zhou, D., Parkes, L., Larsen, B., Adebimpe, A., Kahn, A.E., Gur, R.C., Gur, R.E., Satterthwaite, T.D., Wolf, D.H., Bassett, D.S., 2023. Alprazolam modulates persistence energy during emotion processing in first-degree relatives of individuals with schizophrenia: a network control study. Mol. Psychiatry 28 (8), 3314–3323. https://doi.org/10.1038/s41380-023-02121-z.
Marusak, H.A., Calhoun, V.D., Brown, S., Crespo, L.M., Sala-Hamrick, K., Gotlib, I.H., Thomason, M.E., 2017. Dynamic functional connectivity of neurocognitive networks in children. Hum. Brain Mapp. 38 (1), 97–108. https://doi.org/10.1002/hbm.23346.
Marusak, H.A., Elrahal, F., Peters, C.A., Kundu, P., Lombardo, M.V., Calhoun, V.D., Goldberg, E.K., Cohen, C., Taub, J.W., Rabinak, C.A., 2018. Mindfulness and dynamic functional neural connectivity in children and adolescents. Behav. Brain Res. 336, 211–218. https://doi.org/10.1016/j.bbr.2017.09.010.
Parks, S.M., Stamoulis, C.. Next-generation Neural Data Analysis (NGNDA) platform [Computer software]. https://github.com/cstamoulis1/Next-Generation-Neur-al-Data-Analysis-NGNDA.
Vandenberghe, R., Gitelman, D.R., Parrish, T.B., Mesulam, M.M., 2001. Functional specificity of superior parietal mediation of spatial shifting. Neuroimage 14 (3), 661–673.
Ye, J., Tejavibulya, L., Dai, W., Cope, L.M., Hardee, J.E., Heitzeg, M.M., Lichenstein, S., Yip, S.W., Banaschewski, T., Baker, G.J., Bokde, A.L.W., Brühl, R., Desrivières, S., Flor, H., Gowland, P., Grigis, A., Heinz, A., Martinot, J.L., Paillère Martinot, M.L., Artiges, E., … Scheinost, D. (2024). Variation in moment-to-moment brain state engagement changes across development and contributes to individual differences in executive function. bioRxiv., 2024.09.06.611627. 10.1101/2024.09.06.611627.